Int. J. Electrochem. Sci., 13 **(2018)** 11795 – 11807, doi: 10.20964/2018.12.04

International Journal of
ELECTROCHEMICAL
SCIENCE
www.electrochemsci.org

Electrochemistry of Zr (IV) in molten LiCl–KCl–K_2ZrF_6 System

Chunyue Li, Wei Han, Mei Li, Wei Wang, Xiaoguang Yang[*]

Key Laboratory of Superlight Materials and Surface Technology, Ministry of Education, College of Material Science and Chemical Engineering, Harbin Engineering University, Harbin 150001, P. R. China
[*]E-mail: yxg1122@163.com

Received: 10 April 2018 / *Accepted:* 8 September 2018 / *Published:* 5 November 2018

The electrochemical behaviors of Zr (IV) in the molten LiCl–KCl–K_2ZrF_6 system were investigated on tungsten and copper electrodes at 993 K respectively. By electrochemical tests including cyclic voltammetry, square wave voltammetry, chronopotentiometry and open circuit chronopotentiometry. Zr (IV) was reduced to Zr (0) in two steps with two electrons transfer in each one. The diffusion coefficient of Zr (IV) was 5.01×10^{-5} cm^2/s examined by cyclic voltammetry in the molten salts. The electrochemical signal of Cu–Zr intermetallic compound was detected at -1.0 V(vs. Ag/AgCl). Cu_5Zr, $Cu_{51}Zr_{14}$ and Cu_8Zr_3 were obtained by galvanostatic electrolysis at 0.05 A for 20 h. These intermetallic compounds were characterized by X–ray diffraction analysis (XRD) and scanning electron microscopy with energy dispersive spectrum (SEM–EDS). In this work we provided an efficient way to prepare Cu–Zr intermetallic compounds.

Keywords: Zirconium, Copper, Electrochemical test, Galvanostatic electrolysis, Intermetallic compounds

1. INTRODUCTION

Advantages of nuclear power, such as safety, reliability and economy, are closely related to the properties of the cladding material. Zirconium is an essential recyclable nuclear cladding material for its low neutron absorption cross–section and corrosion resistance in the nuclear industry [1]. Metal zirconium has excellent properties, such as high specific strength, good mechanical properties. Zirconium alloys have predominant corrosion resistance and sufficient thermal stability hence they are ideal materials for nuclear fuel cladding and other reactor devices in the process of nuclear production [2–3]. Popularly, there are basically two ways, metal thermal reduction and molten salt electrolysis, to extract zirconium from spent nuclear fuel. The molten salt electrolysis is an effective method for preparing high–melting point metals and their alloys [4]. Most molten salts have good thermal stability

over a range of temperatures, and in general, they can be employed at temperatures from 373 K to 1373 K (even higher according to the actual need). Due to the lower melting point of the chloride salts compared to the fluorides, the chloride molten salt electrolysis was selected in this study to extract zirconium.

Because $ZrCl_4$ is easy to sublimate when the temperature is higher than 300℃, it will go up into the gas phase mostly if it is added into the heated molten salts directly. Moreover, Zr (IV) sources such as $ZrCl_4$ and ZrF_4 are more expensive than K_2ZrF_6, hence K_2ZrF_6 was used to prepare zirconium in this work.

Electrochemical behaviors of Zr (IV) in the molten salts have been discussed by various methods such as cyclic voltammetry (CV), square wave voltammetry (SWV), chronopotentiometry (CP) and open circuit chronopotentiometry (OCP). Chen et al. [4] have reported that the reaction mechanism of Zr (IV) to Zr (0) was following a two–step electrons transfer and two electrons per step in the molten LiCl–KCl–K_2ZrF_6 system at molybdenum electrode. In order to extract zirconium from spent nuclear fuel, a few active electrodes, for instance, copper, aluminum, zinc and nickel have been applied in the molten salt in the temperature range of 450 to 750℃ [5-10]. Gibilaro et al. [11] have reported that Cu–Zr intermetallic compounds such as Cu_9Zr_2, $Cu_{51}Zr_{14}$, $CuZr_2$ were found on the Cu electrode surface in the LiF–CaF_2–ZrF_4 molten salts system. However, no research has been reported about Cu–Zr alloys in the LiCl–KCl–K_2ZrF_6 system with the copper used as the active electrode.

Because the copper electrode is easily available and non–toxic [12], it was introduced to the molten salts to extract zirconium by forming Cu–Zr intermetallic compounds in this work. The electrochemical signals of copper–zirconium intermetallic compounds were detected by CVs, SWVs, CPs, OCPs and then electrolytic products were characterized by X–ray diffraction (XRD) and scanning electron microscopy with energy dispersive spectrum (SEM–EDS). In this paper we try to provide a new method to obtain Cu–Zr alloys in the LiCl–KCl–K_2ZrF_6 system at low cost.

2. EXPERIMENTAL

2.1 Electrochemical apparatus and chemicals

The experimental instrument in this research is shown in Fig.1. The LiCl–KCl (LiCl:KCl = 38:45, Sinopharm Chemical Reagent Co., Ltd.) molten salts were used in a three–electrode electrochemical cell. A thermocouple was employed to measure the temperature. A tungsten wire (Ø 0.5mm, 99.95% purity) was chosen as the working electrode (WE) for investigating electrochemical behaviors of Zr (IV) and a copper wire (Ø 1.5mm, 99.99% purity) was selected as another working electrode to detect the electrochemical signals of Cu–Zr intermetallic compounds. The counter electrode (CE) was a graphite rod (Ø 6mm, spectroscopically pure). The reference electrode (RE) was made of a silver wire (Ø 1mm) together with the LiCl–KCl–AgCl system. K_2ZrF_6 was selected as the Zr (IV) source, which was provided by Tianjin Institute of Guang Fu Chemical rehabilitation

(analytical purity, 98.0 % purity). In this work, all the equipment was protected by high purity of argon.

Experimental chemicals were analytically pure and dried. The eutectic salt LiCl–KCl had been dried for 24 h at 573 K, and then it was used as electrolytic solvents. The working electrodes were polished by SiC paper and cleaned in dilute hydrochloric by ultrasonic cleaning. The effective WE superficial area was determined by measuring the immersion depth of the electrode in the molten salts. All the experimental operations were carried out in glove box to ensure the anaerobic environment during the experiment. Electrochemical detections were controlled by Autolab PGSTAT 302N (Metrohm, Ltd) and the data were processed by NOVA 1.10 software.

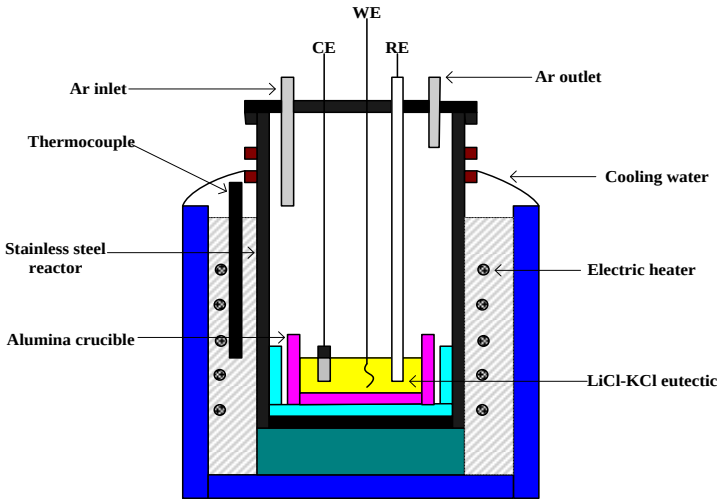

Figure 1. Schematic of the reaction device

2.2 Methods

In order to remove residual water and other impurities contained in the LiCl–KCl eutectic salt thoroughly, pre–electrolysis was applied at -2.0 V(vs. Ag/AgCl) for 4 h at 773 K until the residual current was reduced to less than 5 mA, as is illustrated in Fig. 2. After pre–electrolysis, a certain amount of K_2ZrF_6 was added into the molten salt system as the source of Zr (IV).

Then a tungsten wire was inserted into the molten salts as the working electrode. For investigating electrochemical behaviors of Zr (IV) on tungsten electrode, several electrochemical tests were carried out, such as CVs, SWVs, CPs and OCPs in the temperature range of 773~993 K. The scanning speed of the cyclic voltammetry was 0.1 V/s, and the scanning potential range was from 0 to -2.65 V(vs. Ag/AgCl). Square-wave voltammograms with a step potential of 1 mV and frequencies of 10–25 Hz were adopted. Time periods for chronopotentiometry and open circuit chronopotentiometry both were 25 s. After testing the electrochemical behaviors of zirconium ions on the tungsten electrode, the electrolyte was replaced. Later, a copper electrode (as WE) was inserted into the new electrolyte while the other experimental conditions remain same. Similarly, the electrochemical methods like CVs, SWVs, CPs and OCPs were applied to examine the electrochemical behaviors Zr (IV) on Cu working electrode at 993K. Galvanostatic electrolysis was conducted at 0.05 A for 10 h and

20 h, respectively. Finally, electrolytic products were characterized by XRD (Multi Flex TTR III, Rigaku Industrial Corp. Ltd.) and SEM–EDS (Hitachi SU-70, Japan; EDS: Bruker XFlash Detector 6/60, Germany).

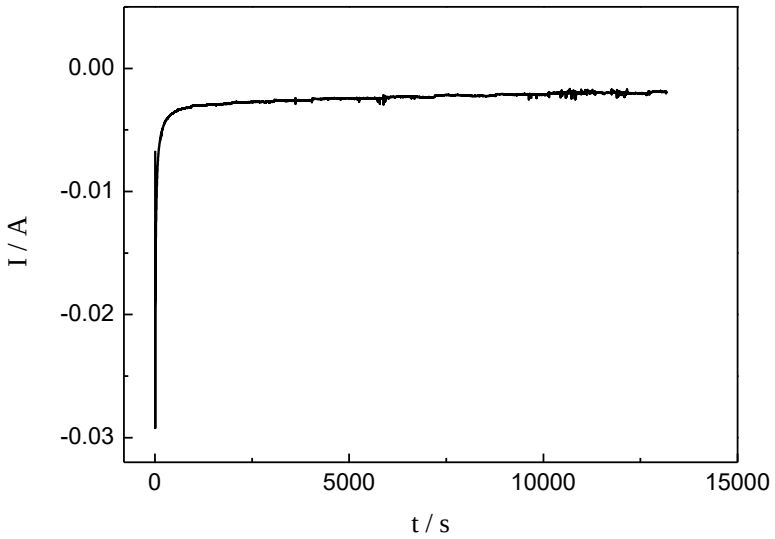

Figure 2. Pre-electrolysis at -2.0 V for 4 h under 773 K. Working electrode, tungsten wire (Ø 0.5mm, 99.95 % purity); counter electrode, vitreous carbon; reference electrode, Ag/AgCl.

3. RESULTS AND DISCUSSION

3.1. Cyclic Voltammetry of K_2ZrF_6 in the LiCl–KCl eutectic salt

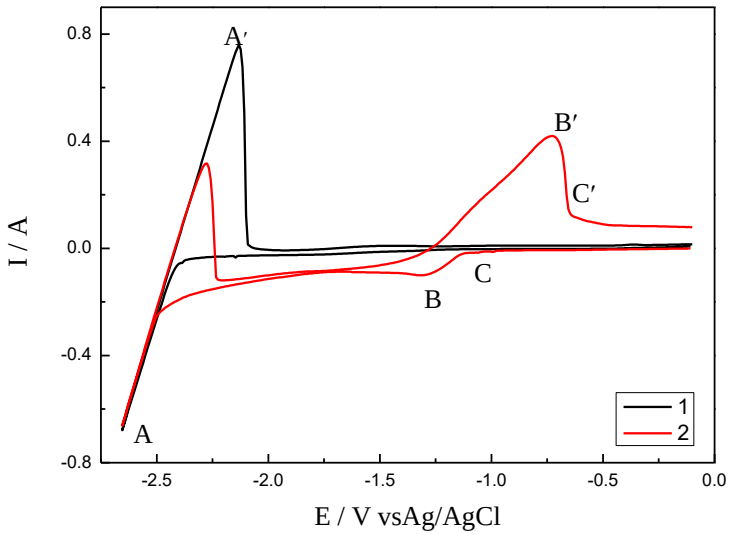

Figure 3. CVs of LiCl–KCl (curve 1) and LiCl–KCl–3.49 wt.% K_2ZrF_6 (curve 2) on tungsten working electrode at 993 K. Scan rate, 100 mV/s. Working electrode, W (0.3454 cm^2); counter electrode, vitreous carbon; reference electrode, Ag/AgCl.

Fig. 3 shows a group of CVs with 0.1V/s on tungsten electrode at 993 K, curve 1 and curve 2 represent before and after the introduction of 3.49 wt.% K_2ZrF_6 to the melt with scanning potential range from 0 to -2.65 V(vs. Ag/AgCl), respectively. In curve 1, the cathodic peak A and the corresponding anodic peak A' are redox peaks of lithium. In curve 2, the cathodic peak C at -0.9 V(vs. Ag/AgCl) may be related to the reduction of Zr (IV)/Zr (II), which corresponds to the following reaction, $Zr\ (IV) + 2e \rightarrow Zr\ (II)$. And another cathodic peak B at -1.25 V(vs. Ag/AgCl) may be corresponding to $Zr\ (II) + 2e \rightarrow Zr\ (0)$. These results are consistent with Xu et. al. [13] in LiCl–KCl–K_2ZrF_6 system.

CVs of LiCl–KCl–1.0 wt.% K_2ZrF_6 with scan rate from 0.02 to 0.08 V/s are shown in Fig. 4(a). To clearly observe the potentials of each pair of redox peaks, cyclic voltammograms with different terminated potentials were used. Fig. 4(b) represents cyclic voltammograms of different negative vertex potentials on tungsten electrode. It can be seen from Fig. 4(b), the first cathodic electrochemical signal occurs at -0.9 V(vs. Ag/AgCl), and the second signal appears at -1.25 V(vs. Ag/AgCl). As the scanning potential shifts towards the negative direction, the electrochemical signals are strengthened. Fig. 4(c) shows that CVs of LiCl–KCl (curve 1) with 100 mV/s and LiCl–KCl–2.0 wt.% K_2ZrF_6 (curve 2) vs. scanning speed range of 10–60 mV/s on copper electrode at 993 K. The reaction mechanism of Zr (IV) to Zr (0) in the molten salts at 993K may be considered as Zr (IV)/Zr (II) at -0.9 V(vs. Ag/AgCl) and Zr (II)/Zr (0) at -1.25 V(vs. Ag/AgCl), respectively.

Zr (IV)/Zr (II) and Zr (II)/Zr (0) may be related to the peaks of C and B in Fig. 4. The cathodic peak potential of B or C is not dependent on the sweep rate. It can be concluded that the reduction processes of Zr (II)/Zr (0) and Zr (IV)/Zr (II) are both reversible (or quasi–reversible). In curve 2 of Fig. 4(c), except the electrochemical signals of copper and Zr, new redox peaks HH' appear obviously, which may be relevant to one or more intermetallic compounds between Cu and Zr.

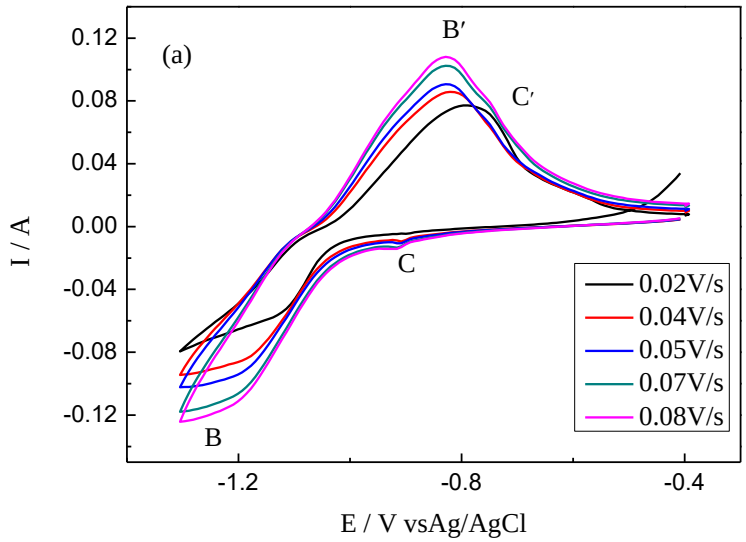

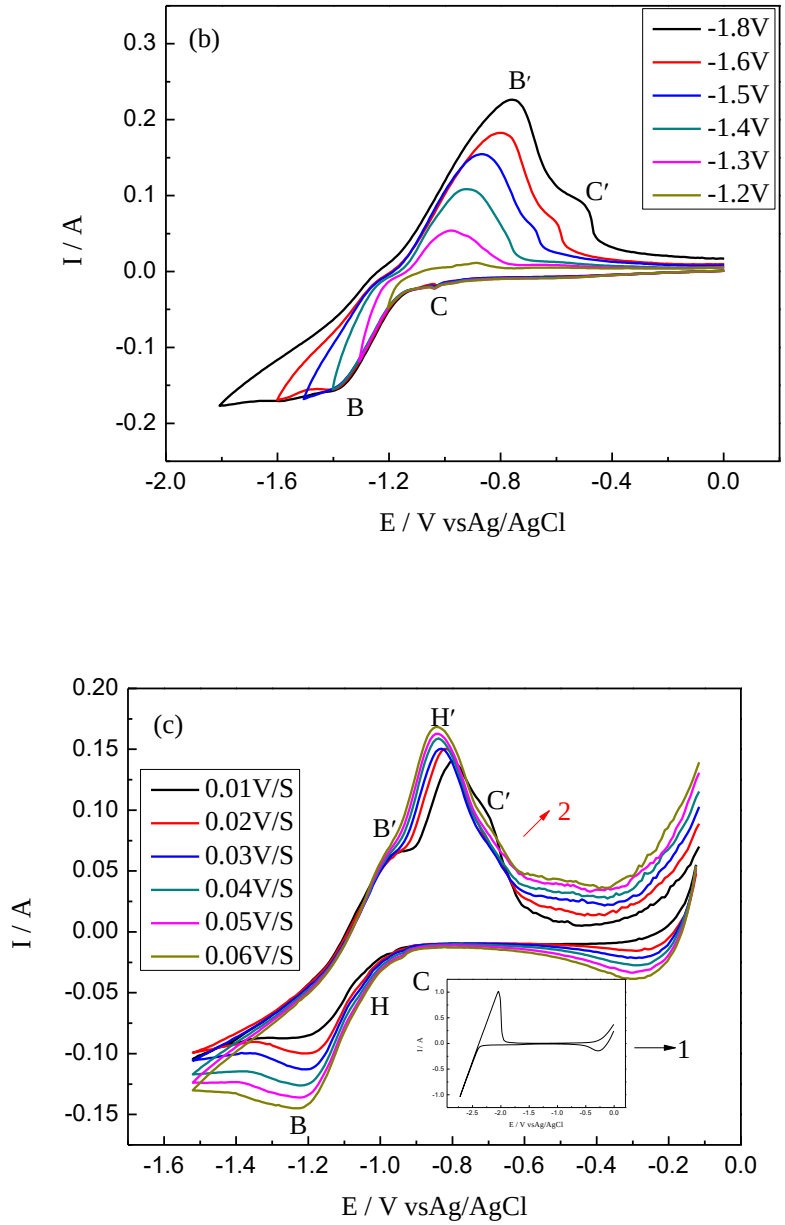

Figure 4. (a) CVs of LiCl–KCl–1.0 wt.% K_2ZrF_6 within scan rates among 20–80 mV/s at 993K. Working electrode, W (0.3454 cm^2); counter electrode, vitreous carbon; reference electrode, Ag/AgCl. (b) CVs of LiCl–KCl–3.0 wt.% K_2ZrF_6 at 993K with scan potentials from -1.8 to -1.2 V(vs. Ag/AgCl). (c) CVs of LiCl–KCl (curve 1) with 100 mV/s and LiCl–KCl–2.0 wt.% K_2ZrF_6 (curve 2) with scan range of 10–60 mV/s at 993K. Working electrode, Cu (0.9404 cm^2); counter electrode, vitreous carbon; reference electrode, Ag/AgCl.

Moreover, the relationship between scan rate and peak potential/current of the cathodic reactions on tungsten electrode is shown in Fig. 5. It can be seen in Fig. 5(a), the peak potential of C (Zr^{4+} / Zr^{2+}) changes so little with scan rate from 0.02 to 0.08 V/s, hence the reaction of Zr (IV)/Zr (II) may be reversible. Furthermore, the relationship between square root of the sweep rate and peak current is illustrated in Fig. 5(b). As is depicted by Fig. 5(b), the reaction of Zr (IV)/Zr (II) is controlled by diffusion. Therefore, the diffusion coefficient of Zr (IV) in the molten can be calculated

by Eq. (1) [14]. The value of D (Zr^{4+}) at 993 K is from 2.88×10^{-5} to 7.15×10^{-5} cm^2/s, resulting in a mean value of 5.01×10^{-5} cm^2/s.

$$I_P = 0.4463(nF)^{3/2}(RT)^{-1/2}AD^{1/2}C\nu^{1/2} \quad (1)$$

Where I_p is the peak current (A), ν is the scan rate (V/s), C is the molar concentration of Zr (IV) ions (mol/cm^3), D is the diffusion coefficient of Zr (IV) (cm^2/s), A is the immersion area of the W working electrode (cm^2), T is the temperature (T), R is the molar gas constant (8.314 J/mol·K), F is the Faraday constant (96500 C/mol), n is the number of exchanged electrons. Here, n is calculated in section 3.2.

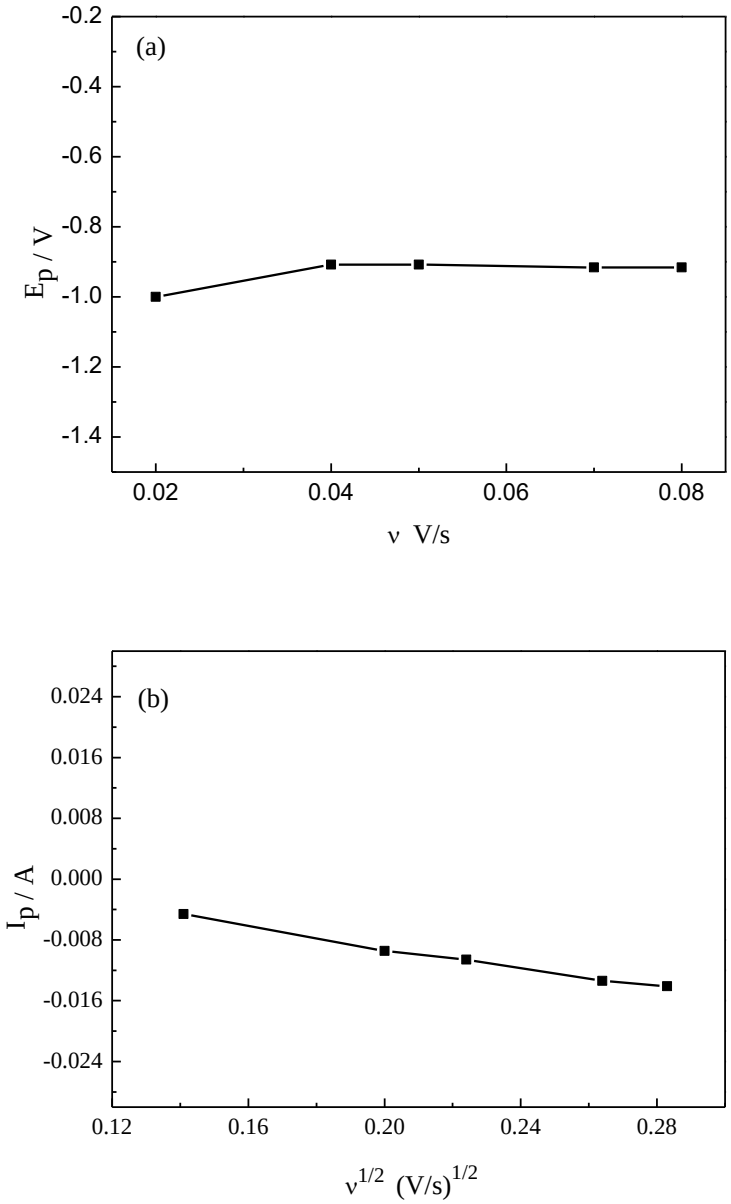

Figure 5. (a) Relationship between a series of scan rate and their peak potentials on W electrode. (b) The peak current changes with the square root of the sweep rate on W electrode.

3.2 Square wave Voltammetry of LiCl–KCl–K_2ZrF_6 system

Fig. 6 reveals square wave voltammograms with different frequencies of Zr (IV) on copper electrode at 993 K. It is clear that apart from B and C, H appears again at -1.0 V(vs. Ag/AgCl). Based on the electrochemical signal at -1.0 V(vs. Ag/AgCl) in CVs, it can be inferred that H is the electrochemical signal of one intermetallic compound. According to Bard and Faulkner [14], the relationship between the number of electrons transferred (n) and half-width of the peak ($W_{1/2}$) should be calculated according to Eq. (2) [1, 4, 13, 15].

$$W_{1/2} = 3.52\frac{nF}{RT} \quad (2)$$

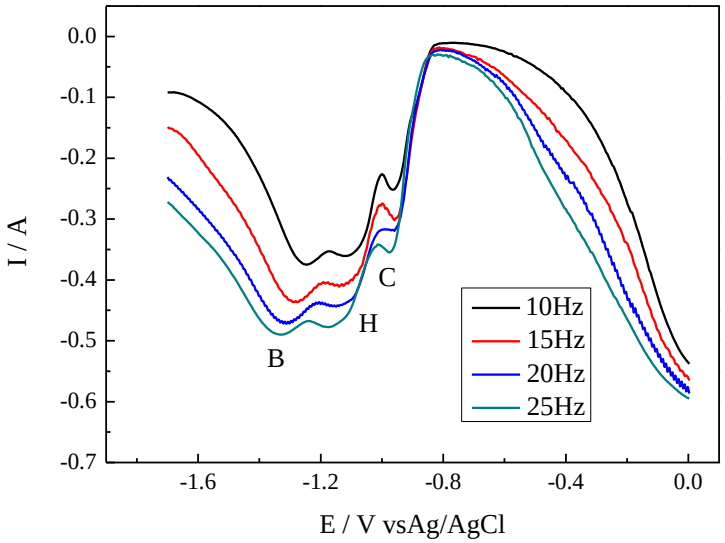

Figure 6. SWVs with different frequencies of Zr (IV) on copper electrode at 993 K. Working electrode, Cu (0.9404 cm^2); counter electrode, vitreous carbon; reference electrode, Ag/AgCl. Potential step: 1 mV.

By Eq. (2), the number of transferred electrons at the B and C peaks was calculated. The number of transferred electrons at B and C is 2, respectively. Therefore, the reaction mechanism of Zr (IV) to Zr (0) is determined in two steps with the exchange of two electrons, respectively. As is shown in Fig. 6, the reaction of Zr (IV) to Zr (0) is consistent with the study of Wu et.al [16]. This result about the reaction mechanism verifies the speculation in section 3.1.

3.3 Chronopotentiometry

To further confirm the reduction mechanism of Zr ions obtained by cyclic voltammetry and square wave voltammetry, chronopotentiometry was applied at 993 K in this work. The reaction progress of Zr (IV)/Zr (II) on tungsten electrode is shown in Fig.7(a) with a series of current from -3.5 to -107 mA. Two potential platforms appear at -0.9 and -1.25V(vs. Ag/AgCl), which are consistent with the results in sections 3.1 and 3.2. Fig. 7(b) shows the reaction platforms of Zr (IV) on copper

electrode, and the current range is from 0.08 to -0.1 A. These plateaus close to -0.9 V and -1.25 V(vs. Ag/AgCl) are corresponding to the reduction processes of Zr (IV)/Zr (II) and Zr (II)/Zr (0). The electrochemical signal at -2.4 V(vs. Ag/AgCl) in Fig. 7(b) is the reduction process of lithium. In Fig. 7(b), there is only one platform of intermetallic compound emerging at -1.0 V(vs. Ag/AgCl). This result may be due to the overlapping of electrochemical signals for different intermetallic compounds.

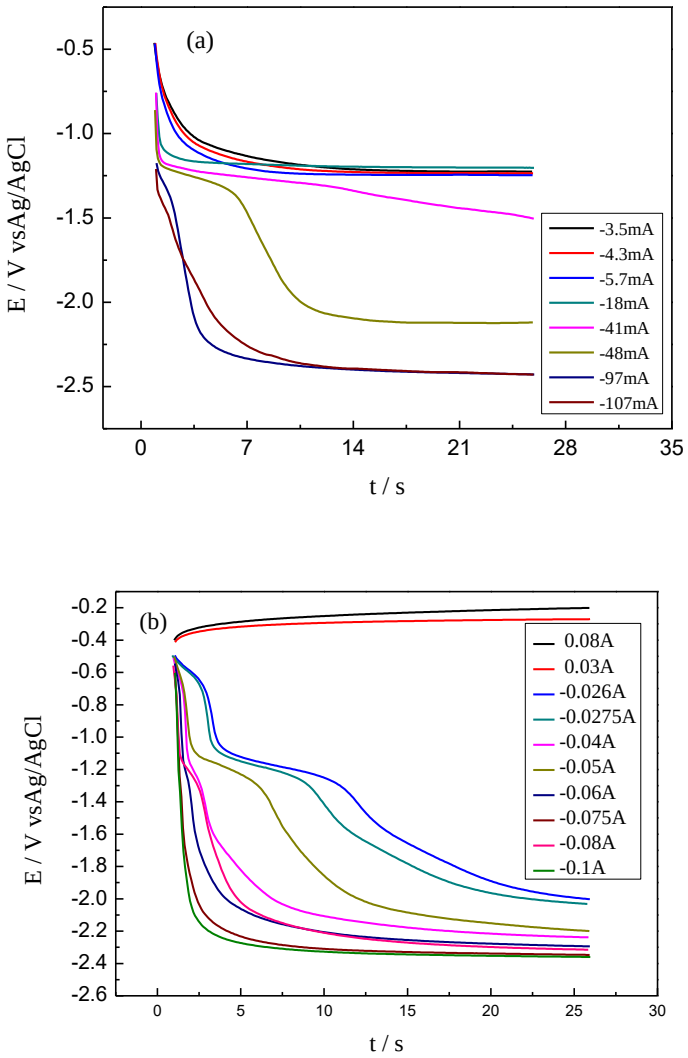

Figure 7. (a) Chronopotentiograms at 993 K with varied currents from -3.5 to -107 mA. Working electrode, W (S=0.3454 cm^2); counter electrode, vitreous carbon; reference electrode, Ag/AgCl. (b) Chronopotentiograms at 993K with varied currents from 8 to -100 mA. Working electrode, Cu (S=0.942 cm^2); counter electrode, vitreous carbon; reference electrode, Ag/AgCl.

3.4 Open circuit chronopotentiometry

Open circuit chronopotentiometry was carried out to investigate the redox mechanism of zirconium by the balance of deposition and dissolution on the surface of the working electrode at 993K in Fig. 8. With deposition for 25 seconds at -2.6 V(vs. Ag/AgCl), the circuit was switched off. Then the zirconium deposited on the Cu working electrode began to dissolve. The first dissolution platform

A at -2.34 V(vs. Ag/AgCl) is related to Li/Li (I), B at -1.1 V(vs. Ag/AgCl) is due to Zr (0)/Zr(II), H at -0.96 V(vs. Ag/AgCl) is belonging to one or more intermetallic compounds, and plateau C at -0.8 V(vs. Ag/AgCl) is according to the process of Zr (II)/Zr (IV). Because it is soluble–soluble, plateau C is not obvious. The subsequent plateaus at about -1.1 and -0.8 V(vs. Ag/AgCl) are corresponded to the two–step oxidation processes which are from Zr (0) to Zr (II) and Zr (II) to Zr (IV).

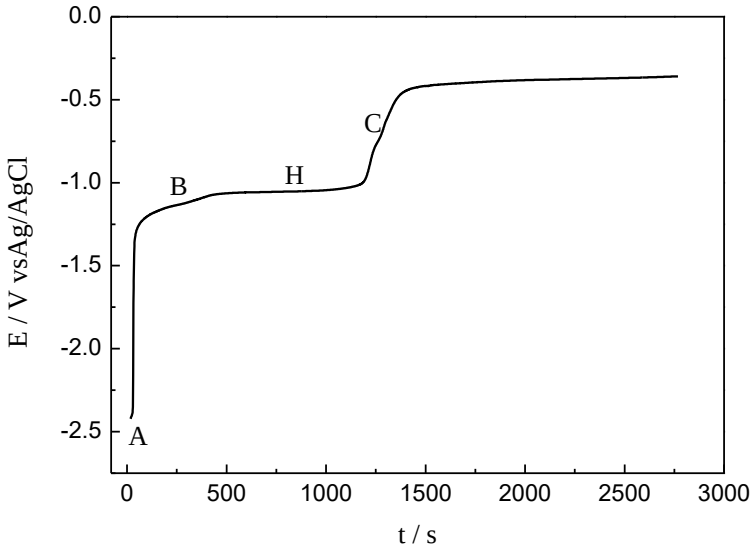

Figure 8. Open circuit chronopotentiometry at 993 K with electrodepositing at –2.5 V for 25 s on the working electrode. Working electrode, Cu (S=0.942 cm^2); counter electrode, vitreous carbon; reference electrode, Ag/AgCl.

3.5 Galvanostatic electrolysis

Electrochemical signals of Cu–Zr intermetallic compounds were not distinct in different electrochemical tests, therefore, potentiostatic electrolysis was vain for this system. So as to ascertain the kind of intermetallic compound on the copper electrode, galvanostatic electrolysis was introduced at 993 K. In order to ensure that the zirconium ion concentration is high enough, 3.0 g K_2ZrF_6 was added into molten salts (83 g) before electrolysis. Electrolysis experiments were conducted using a copper sheet (5 mm × 11 mm) as cathode and a spectrum pure graphite rod as anode. By galvanostatic electrolysis at 0.05 A for 20 h, three kinds of intermetallic compounds (Cu_5Zr, $Cu_{51}Zr_{14}$, and Cu_8Zr_3) were obtained. After electrolysis, the copper electrode was washed by deionized water with its adherent salt eliminated by ultrasonic. According to the Cu–Zr phase diagram [17], six intermetallic compounds are available, i.e. Cu_9Zr_2, $Cu_{51}Zr_{14}$, Cu_8Zr_3, $Cu_{10}Zr_7$, CuZr, $CuZr_2$. Gibilaro [11] has reported three intermetallic compounds (Cu_9Zr_2, $Cu_{51}Zr_{14}$, $CuZr_2$) were detected from the deposition layers in the electroreduction of Zr (IV) on the Cu electrode. In our work, there were three intermetallic compounds observed by SEM–EDS and XRD. Based on Cu–Zr phase diagram [17], Cu–Zr intermetallic compounds are formed at 1158 K at least, but in the present work they were synthesized at 993 K. This can be explained by the micro–area thermal theory [18].

3.6 Characterization of the electrolytic products

In order to characterize electrolytic products, XRD (using Cu Kα radiation at 40 kV and 150 mA) was employed. Fig. 9(a) depicts the XRD pattern on the copper electrode obtained at 0.05 A for 10 h. Diffraction peaks at 43, 50 and 74 degrees are corresponding to Cu, while no Zr (0) is found on the copper electrode. Fig. 9(b) represents the XRD pattern of the copper electrode obtained at 0.05 A for 20 h. The diffraction peaks of the intermetallic compounds are too close to be separated from each other obviously.

Fig. 10 shows a series of SEM images and EDS analysis. Fig. 10(A) reveals that there is no Zr (0) appeared on Cu electrode with electrolysis at 0.05 A for 10 h. However, three Cu_xZr_y intermetallic compounds (Cu_5Zr, $Cu_{51}Zr_{14}$ and Cu_8Zr_3) are detected clearly with electrolysis for 20 h under the same condition, as is depicted by Fig. 10(B – D). This result is consistent with that of XRD.

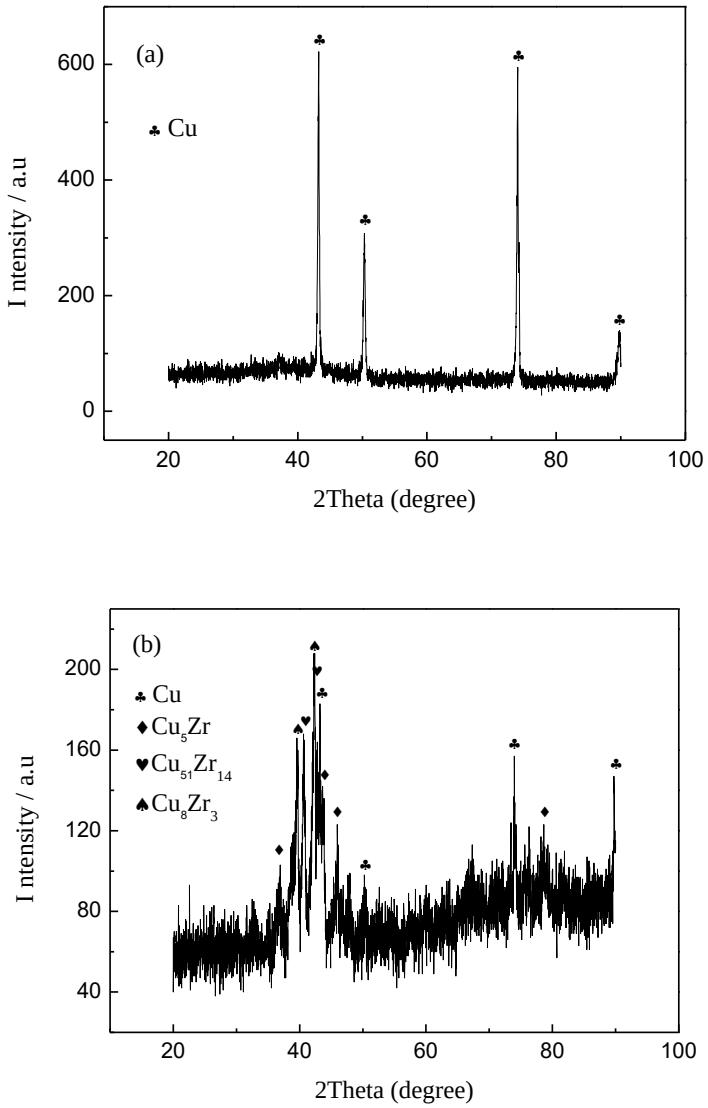

Figure 9. (a) XRD analysis of the copper electrode under 0.05 A at 993 K for 10 h, (b) XRD analysis of the copper electrode under 0.05 A at 993 K for 20 h.

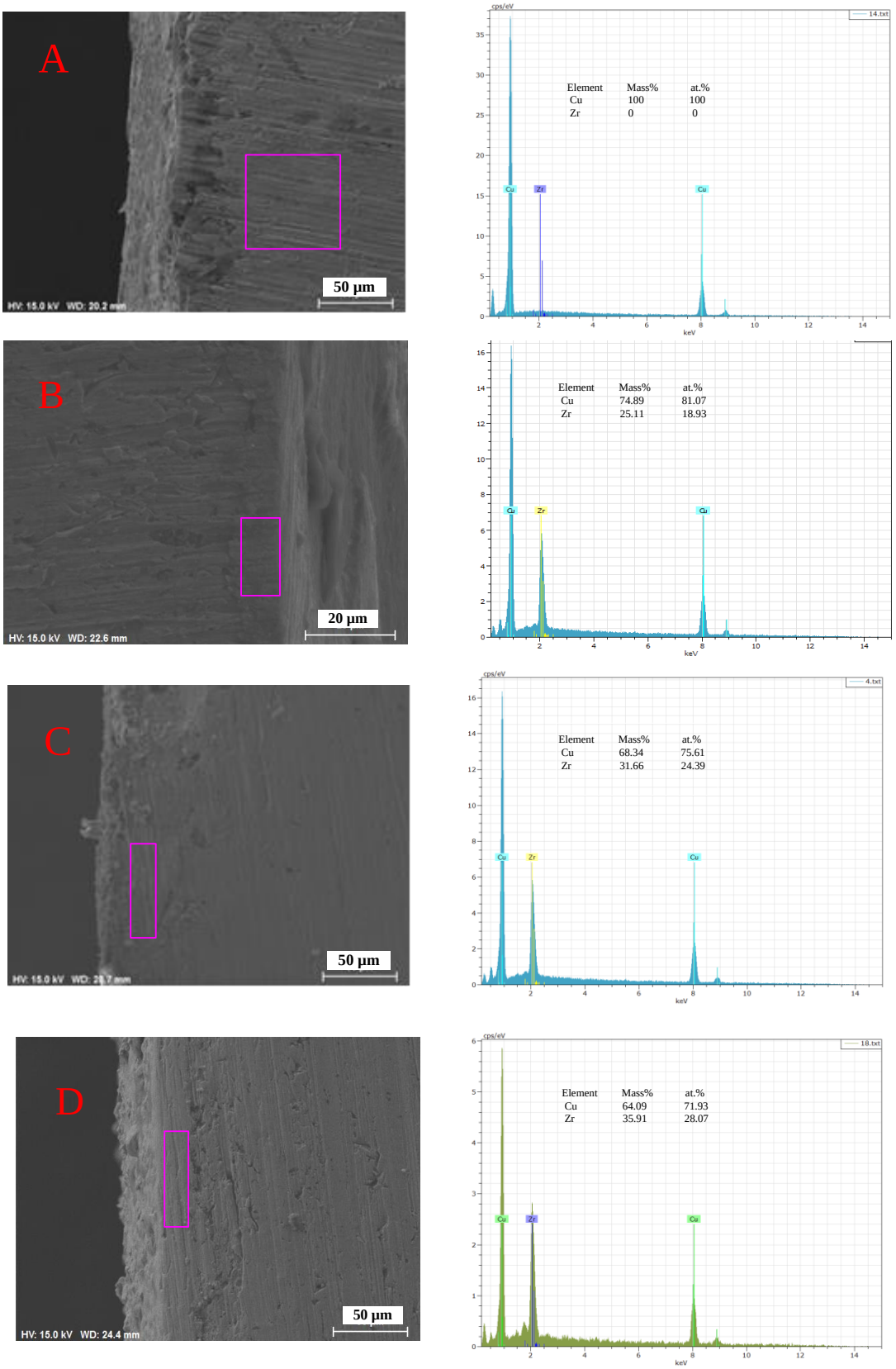

Figure 10. SEM micrographs of a cross section of Cu electrodes at 993 K with galvanostatic electrolysis for 10 h (A) and 20 h (B-D) at 0.05 A, respectively.

4. CONCLUSIONS

In the LiCl–KCl molten salts system, electrochemical behaviors of Zr (IV) were examined on tungsten and copper electrodes by different electrochemical tests (CVs, SWVs, CPs, OCPs) respectively. The electrochemical redox process of Zr (IV) to Zr (0) was found as a two–step process with two electrons transfer per step. The diffusion coefficient of Zr (IV) in the LiCl–KCl eutectic melt at 993 K was 5.01×10^{-5} cm^2/s by cyclic voltammogram. Electrochemical signal was found at –1.0 V(vs. Ag/AgCl), which may be due to intermetallic compounds. By galvanostatic electrolysis at 0.05 A for 20 h, three intermetallic compounds (Cu_5Zr, $Cu_{51}Zr_{14}$ and Cu_8Zr_3) were obtained on the copper electrode, characterized by XRD and SEM.

ACKNOWLEDGMENTS
The work was financially supported by the National Natural Science foundation of China (NSFC) Grant No.21790373, the Major Research plan of the National Natural Science Foundation of China (No.91326113), and the Fundamental Research funds for the Central Universities (No.HEUCFP201793).

References

1. L. Xu, Y. Xiao, Q. Xu, A. V. Sandwijk, J. Li, Z. Zhao, Q. S and Y. Yang, *Rsc Adv*., 488 (2017) 295.
2. M. Iizuka, K. Kinoshita and T. Koyama, Modeling of anodic dissolution of U-Pu-Zr ternary alloy in the molten LiCl-KCl electrolyte, 11th International Conference on High Temperature materials Chemistry, Tokyo, JAPAN, 2005, 427.
3. H. Groult, A. Barhoun, H. El. Ghallali, S. Borensztjan and F. Lantelme, *J. Electrochem. Soc*., 155 (2008) E19.
4. Z. Chen, Y. J. Li and S. J. Li, *J. Alloys Compd*., 509 (2011) 5958.
5. M. Ueda, T. Teshima, H. Matsushima and T. Ohtsuka, *J. Solid State Chem*., 19 (2015) 3485.
6. V. T. Witusiewicz and F. Sommer, *J. Alloys Compd*., 289 (1999) 152.
7. W. F. Zhu, Q. Luo, J. Y. Zhang and Q. Li, *J. Alloys Compd*., 731 (2018) 784.
8. K. Itoh, J. Saida and T. Otomo, *J. Alloys Compd*., 732 (2018) 585.
9. K. V. Yang, Y. J. Shi, F. Palm, X. H. Wu and P. Rometsch, *Scripta Mater*., 145 (2018) 113.
10. J. J. Luo, T. Yin, B. Y. Bai, J. Y. Zhang and Z. H. Zhang, Experimental Investigation of Zn-Zr Binary of Zr-Rich Part Phase Diagram,TMS 2015 144th Annual Meeting & Exhibition, California, America, 2015, 115.
11. M. Gibilaro, L. Massot, P. Chamelot, L. Cassayre and P. Taxil, *Electrochim Acta*, 95 (2013) 185.
12. Y. Q. Cai, H. X. Liu, Q. Xu, Q. S. Song and L. Xu, *Electrochim. Acta*, 161 (2015) 177.
13. L. Xu, Y. P. Xiao, Q. Xu, Q. S. Song and Y. X. Yang, *Int. J. Electrochem. Sci*., 12 (2017) 6393.
14. A. J. Bard and L. R. Faulkner, Electrochemical Methods: fundamentals and applications, Wiley & Sons Inc, (2011) New York, America.
15. J. Park, S. Choi, S. Sohn, K. Kim and I. S. Hwang, *J. Electrochem. Soc*., 161 (2014) H97.
16. Y. K. Wu, Z. G. Xu, S. Chen, L. J. Wang and G. X. Li, *Rare Metals*, 30 (2011) 8.
17. W.G. Moffatt, The handbook of binary phase diagrams, (1976) Genium Pub, New York, America.
18. T. Watanabe, Nano-plating: microstructure control theory of plated film and data base of plated film microstructure, Elsevier, (2004), Amsterdam, Netherlands.